SUPPLEMENTARY MATERIAL

ADDITIONAL RESULTS

Primary congenital or adulthood-onset lymphedema is absent in adult *Adm*^{AM} haploinsufficient mice

To evaluate the potential role for endogenously produced AM in the pathogenesis of primary lymphedema, we examined adult wild type and *Adm*$^{AM+/\Delta}$ mice under physiological, i.e. unchallenged, conditions. Upon histological examination, the skin from mice in both groups appeared to be normal, as assessed by haematoxylin and eosin or Azan staining (Supplementary Figure S1a-b). The thickness of the epidermis (Supplementary Figure S1a, c), as well as the collagen matrix organisation (Supplementary Figure S1b), in the skin of adult *Adm*$^{AM+/\Delta}$ mice were grossly comparable to that of wild type mice; although moderate increase in the cellularity (Supplementary Figure S1a) and collagen fiber density (Supplementary Figure S1d) were found in the dermis of the *Adm*^{AM} haploinsufficient animals. The marked increase in collagen content reflects changes associated with lymphedema (Rutkowski *et al.*, 2010; Wilson *et al.*, 2004; Wu *et al.*, 2011). The pronounced changes in collagen fibers density were found in the skin of a few (two amongst 13 examined) adult *Adm*$^{AM+/\Delta}$ mice upon histological analysis (not shown). Immunohistochemistry using lymphatic and blood endothelium markers was performed to distinguish between microvessel phenotypes, and to analyse their morphological properties, such as number and diameter (Supplementary Figure S1e). We found that lymphatic and blood microvessels morphology was grossly unaltered in *Adm*$^{AM+/\Delta}$, when compared to the wild type, animals (Supplementary Figure S1f-g). Furthermore, no accumulation of fibrin, used as a marker of plasma filtration and vascular leakage (Chen *et al.*, 2005), was seen in the skin of

mice from both groups (Supplementary Figure S1h). Finally, the function of the collecting lymphatic vessels in the lower limbs of the adult wild type or $Adm^{AM+/\Delta}$ animals was not impaired, as analysed by performing regional lymphangiography (Supplementary Figure S1i), followed by the subsequent visualization and measurement of dye accumulation in inguinal lymph nodes (Supplementary Figure S1j-k). Our gross findings in the skin tissue from wild type and Adm^{AM} haploinsufficient mice are summarized in the Supplementary Table S1. In summary, no obvious morphological abnormalities, including histopathological changes characteristic of lymphedema, or edema, were found in either wild type or $Adm^{AM+/\Delta}$ animals (Supplementary Table S1 and Supplementary Figure S1). Based on these findings, we concluded that under normal physiological conditions, Adm^{AM} haploinsufficiency (resulting in AM deficiency) caused neither congenital nor adulthood-onset primary lymphedema in our *in vivo* model.

CLR generates functional adrenomedullin receptors in primary endothelial cells in vitro

The glycosylation status of CLR (previously termed CRLR) is critical to its properties: only mature, fully (terminally) glycosylated CLR species are expressed at the cell surface and selectively recognized by its ligands (Hilairet *et al.*, 2001; McLatchie *et al.*, 1998). Terminally- as well as core-glycosylated CLR species were expressed in cultured MVLEC (Supplementary Figure S10a-e). Terminal glycosylation and subsequent transport of CLR to the cell surface is determined by its co-expression with receptor-activity modifying proteins (RAMPs) (McLatchie *et al.*, 1998). The presence of the cell-surface expressed (terminally glycosylated) form of CLR in MVLEC was accompanied by the expression of *RAMP2* and *3* mRNAs (Figure 5b in the main text; Supplementary Figure S9), suggesting that endogenous CLR generates AM receptors AM1 or AM2, or both, in these cells. Next, we performed an internalization study using synthetic AM and $AM_{22\text{-}52}$ (a truncated form of AM, which acts as AM receptor antagonist)

(Poyner *et al.*, 2002). Rapid (within 5-15 min after stimulation) agonist-mediated CLR internalization occurred in MVLEC in response to AM and AM_{22-52} counteracted this response (Supplementary Figure S10f), suggesting that AM interacts directly with endogenous CLR in MVLEC. Together, our results (Figure 5; Supplementary Figures S9 and S10) suggest that both *in vivo* and *in vitro* CLR protein is expressed in lymphatic endothelium, where upon co-expression with RAMPs 2 and 3 it generates functional (fully glycosylated and cell surface expressed) endogenous AM receptors.

SUPPLEMENTARY METHODS

Lymphangiography and Evans blue accumulation assays

In order to assess lymphatic vessel function and lymphatic fluid transport and uptake, two days after the incision wounding mice were anaesthetized with pentobarbital and the 2% Evans blue dye in the saline (50µl) was injected into the footpads subdermally. Ten minutes after the injection, lymphatic vessels were observed under the microscope. Twenty four hours after the dye was administered, inguinal lymph nodes were excised, homogenised in 1.5ml of formamide and Evans blue accumulation was measured as previously described (Gon *et al.*, 2005). In brief, Evans blue was extracted by incubating the samples at 70ºC for 24h, and the absorbance was measured by dual-wave-length spectrophotometer (620 nm and 740 nm). The following formula was used to correct optical densities (E) for contamination with heme pigments: $E620_{(corrected)} = E620_{(raw)} - (1.426 \times E740_{(raw)} + 0.030)$.

In order to assess blood vessel leakage and permeability, Evans blue accumulation assay was performed as described elsewhere (Parikh *et al.*, 2006). In brief, mice were anesthetized and 2% Evans blue in the saline (50µl) was then injected into the tail vein. Ten minutes later, mice were

sacrificed and perfused with PBS with 2mM EDTA for 10 min through a cannula placed in the right ventricle. After this, the outflow from the vena cava was observed to be clear, confirming that blood (and intravascular Evans blue) had been flushed out of the circulation. Washout of intravascular contents was also confirmed histologically. Hind limb skin at the site of surgery was then harvested, homogenised and Evans blue content was measured as described above.

Histology, immunostaining and image analysis

Immunohistochemistry and immunofluorescence were done according to the previously described methods (Nikitenko *et al.*, 2006a; Nikitenko *et al.*, 2006b). Mouse Lyve-1, endomucin, proliferating cell nuclear antigen (Pcna), fibrin (used as a marker of plasma filtration and vascular leakage) (Chen *et al.*, 2005), human LYVE-1 and CD34 were detected using antibodies from Acris (Herford, Germany), Santa Cruz Biotechnology (Santa Cruz, CA), Accurate Chemical and Scientific Corporation (Westbury, NY), DAKO (Ely, UK) and Novus Biologicals (Littleton, CO). Rabbit polyclonal antibody LN1436 was raised against synthetic peptide corresponding to 15 amino acid residues at the extreme COOH terminus of human CLR protein (accession numbers AAC41994 and AAA62158) and characterized previously (Nikitenko *et al.*, 2006a). Anti-human podoplanin antibody was a gift from Dr. Gert Zimmer (Institute für Virologie, Tierärztliche Hochschule Hannover, Germany (Zimmer *et al.*, 1999)).

In brief, for immunohistochemistry, after de-paraffinization and rehydration, pre-blocking and incubation with primary antibody overnight at 4ºC, sections were washed and incubated with biotinylated secondary antibody. After subsequent washes and incubation with streptavidin-horse radish peroxidase (HRP) complex using Vectastain ABC-HRP Kit (Vector Labs, Burlingame, UK), all immunohistochemistry reactions were followed by final washes and detection. HRP visualization was performed using diaminobenzidine (DAB) (Vector Labs,

Burlingame, UK). Visualization was carried out with the use of Zeiss Axioshop2 microscope and images were acquired with AxioCam digital camera and AxioVision Software. For double/triple color immunofluorescence, anti-Pcna/anti-Lyve-1 or anti-LYVE-1/anti-CD31/anti-CLR combinations of primary antibodies were used. Appropriate (all raised in donkey) secondary antibodies were conjugated to Alexa Fluor 488, 594 or 647 (Life Technologies, Paisley, UK). Sections were mounted in Vectorshield medium with DAPI, which was used to counterstain cell nuclei. Images were acquired using Perkin Elmer Ultraview Spinning Disc confocal microscope system powered by Volocity Acquisition and captured by built-in EMCCD Hamamatsu C9100-50 ECCD digital camera. All images were subsequently processed using Adobe Photoshop CS3 software. Substitution of primary antibody with isotype-matched IgG, used at appropriate concentrations, served as negative controls to indicate the specificity of the antibodies.

Number of the nuclei per perimeter of lymphatic vessel and number of proliferating lymphatic endothelial cell nuclei were quantified manually (at least fifty vessels and at least one hundred cells per each experimental group were analyzed).

Primary human endothelial and non-endothelial cells

Microvascular dermal blood and lymphatic endothelial cells were isolated and cultured as previously described (Makinen *et al.*, 2001; Vart *et al.*, 2007; Wang *et al.*, 2004), and characterized by their expression of the pan-endothelial marker CD31, and lymphatic endothelium-specific markers – podoplanin and PROX1 using FACs and/or immunofluorescence, and used at passages 3-7.

Non-endothelial cells were originally obtained from Clonetics or isolated from human tissues (Wang *et al.*, 2004). All primary cells have been routinely tested and authenticated and cultured according to the manufacturer's instructions or previously described methods.

Peptides, antagonists and growth factors. Synthetic human AM, CGRP and the antagonists AM_{22-52} and $CGRP_{8-37}$ were obtained from the Bachem (St Helens, United Kingdom).

Deglycosylation experiments. Deglycosylation experiments were done using endoglycosidases F and H (Roche) and according to the supplier's protocols (Roche, Lewes, United Kingdom) and as previously described (Nikitenko *et al.*, 2006a) before SDS-PAGE and immunoblotting.

SDS-PAGE and immunoblotting. Protein lysates from cells were obtained and subjected to SDS-PAGE and immunoblotting as described previously (Nikitenko *et al.*, 2006a).

GeneChip® Human Genome Array analysis. GeneChip® HG-U133Av2 arrays were processed using total RNA obtained from the cells cultured *in vitro* by employing previously established methods (Henderson *et al.*, 2005; Wang *et al.*, 2004), and the data were deposited at the Expression Project for Oncology expO (http://www.intgen.org/expo.cfm) via the NCBI GEO repository ((Edgar *et al.*, 2002); http://www.ncbi.nlm.nih.gov/projects/geo; accession number GSE39262).

GeneChip® Human Genome Array analysis was performed using Affymetrix HG-U133Av2 GSE39262 data and compared to public data obtained from the ArrayExpress database (http://www.ebi.ac.uk/arrayexpress/; accession number E-MEXP-66) containing expression data

obtained using RNA from twelve different human microvascular blood (n=6) and lymphatic (n=6) EC cultures and other primary cells (Wang *et al.*, 2004).

Processed gene expression data from all samples were analyzed as previously described (Wang *et al.*, 2004). In brief, for all GeneChip® arrays raw data were pre-processed and normalized using Bioconductor software for R (Gentleman, 2005) and the robust-multiarray algorithm (rma) (Gautier *et al.*, 2004). Normalized expression data for *CALCRL, RAMP 2, RAMP3* and *ACTB* (beta-actin; used as control) were used to calculate mean values ('rma' $\log_2$ expression units) for each individual probe (*CALCRL* mRNA probe 210815_s; *RAMP2* - 205779_at; *RAMP3* - 205326_at; *ACTB* – 200801_x_at) and presented as a heatmap or using dot plot.

SUPPLEMENTARY REFERENCES

Chen J, Somanath PR, Razorenova O *et al.* (2005) Akt1 regulates pathological angiogenesis, vascular maturation and permeability in vivo. *Nat Med* 11:1188-96.

Edgar R, Domrachev M, Lash AE (2002) Gene Expression Omnibus: NCBI gene expression and hybridization array data repository. *Nucleic Acids Res* 30:207-10.

Gautier L, Cope L, Bolstad BM *et al.* (2004) affy--analysis of Affymetrix GeneChip data at the probe level. *Bioinformatics* 20:307-15.

Gentleman R (2005) *Bioinformatics and computational biology solutions using R and Bioconductor*. Springer Science+Business Media: New York, xix, 473 p.

Gon Y, Wood MR, Kiosses WB *et al.* (2005) S1P3 receptor-induced reorganization of epithelial tight junctions compromises lung barrier integrity and is potentiated by TNF. *Proc Natl Acad Sci U S A* 102:9270-5.

Henderson SR, Guiliano D, Presneau N *et al.* (2005) A molecular map of mesenchymal tumors. *Genome Biol* 6:R76.

Hilairet S, Foord SM, Marshall FH *et al.* (2001) Protein-protein interaction and not glycosylation determines the binding selectivity of heterodimers between the calcitonin receptor-like receptor and the receptor activity-modifying proteins. *J Biol Chem* 276:29575-81.

Makinen T, Veikkola T, Mustjoki S *et al.* (2001) Isolated lymphatic endothelial cells transduce growth, survival and migratory signals via the VEGF-C/D receptor VEGFR-3. *The EMBO Journal* 20:4762-73.

McLatchie LM, Fraser NJ, Main MJ *et al.* (1998) RAMPs regulate the transport and ligand specificity of the calcitonin-receptor-like receptor. *Nature* 393:333-9.

Nikitenko LL, Blucher N, Fox SB *et al.* (2006a) Adrenomedullin and CGRP interact with endogenous calcitonin-receptor-like receptor in endothelial cells and induce its desensitisation by different mechanisms. *J Cell Sci* 119:910-22.

Nikitenko LL, Cross T, Campo L *et al.* (2006b) Expression of terminally glycosylated calcitonin receptor-like receptor in uterine leiomyoma: endothelial phenotype and association with microvascular density. *Clin Cancer Res* 12:5648-58.

Parikh SM, Mammoto T, Schultz A *et al.* (2006) Excess circulating angiopoietin-2 may contribute to pulmonary vascular leak in sepsis in humans. *PLoS Med* 3:e46.

Poyner DR, Sexton PM, Marshall I *et al.* (2002) International Union of Pharmacology. XXXII. The mammalian calcitonin gene-related peptides, adrenomedullin, amylin, and calcitonin receptors. *Pharmacol Rev* 54:233-46.

Rutkowski JM, Markhus CE, Gyenge CC *et al.* (2010) Dermal collagen and lipid deposition correlate with tissue swelling and hydraulic conductivity in murine primary lymphedema. *The American Journal of Pathology* 176:1122-9.

Vart RJ, Nikitenko LL, Lagos D *et al.* (2007) Kaposi's sarcoma-associated herpesvirus-encoded interleukin-6 and G-protein-coupled receptor regulate angiopoietin-2 expression in lymphatic endothelial cells. *Cancer Research* 67:4042-51.

Wang HW, Trotter MW, Lagos D *et al.* (2004) Kaposi sarcoma herpesvirus-induced cellular reprogramming contributes to the lymphatic endothelial gene expression in Kaposi sarcoma. *Nat Genet* 36:687-93.

Wilson SF, Guarner J, Valme AL *et al.* (2004) Histopathologic improvement with lymphedema management, Leogane, Haiti. *Emerging Infectious Diseases* 10:1938-46.

Wu X, Zhuo S, Chen J *et al.* (2011) Real-time in vivo imaging collagen in lymphedematous skin using multiphoton microscopy. *Scanning* 33:463-7.

Zimmer G, Oeffner F, Von Messling V *et al.* (1999) Cloning and characterization of gp36, a human mucin-type glycoprotein preferentially expressed in vascular endothelium. *The Biochemical Journal* 341 (Pt 2):277-84.

Table S1. Characterization of the wild type and *Adm*^{AM} haploinsufficient mice and the summary of the of the gross findings in the skin tissue.

Parameter measured	*Adm*$^{AM+/+}$ (*n*)	*Adm*$^{AM+/\Delta}$ (*n*)
Age (weeks)	8-9	8-9
Weight (g)	22.75±0.83 (*4*)	23.75±0.83 (*4*)
Adm* mRNA in skin, ratio *Adm/Actb mRNA	0.031±0.023 (*3*)	0.031±0.002 [1] (*3*)
AM in plasma, fmol/ml	26.02±1.14 (*9*)	13.92±0.57 [2] (*7*)
PAMP in plasma, fmol/ml	12.51±3.61 (*7*)	17.27±9.61 (*7*)
Epidermis	no obvious differences (*7*)	between two groups (*13*) [3]
Dermis	no obvious differences (*7*)	between two groups (*13*) [3]
Dermal miscrovasculature		
Lymphatic capillaries (Lyve-1 +ve)		
area, %	1.76±0.11 (*4*)	1.57±0.11 (*4*)
number per square mm	58.46±5.67 (*4*)	70.88±6.73 (*4*)
Blood capillaries (Endomucin +ve)		
area, %	1.01±0.18 (*4*)	0.68±0.26 (*4*)
number per square mm	184.76±25.83 (*4*)	158.47±14.58 (*4*)
Subcutis	no obvious differences (*7*)	between two groups (*13*)

Data are presented as mean ± S.D. Number of mice used in each group are shown in brackets, (*n*).
[1] *Adm* gene mutant locus is successfully transcribed in the tissues of an adult *Adm*$^{AM+/\Delta}$ mice, but the introduced stop codon prevents AM biosynthesis, resulting in peptide deficiency, as shown on the Figure 1a.
[2] p value <0.001 [3] Two mice had pronounced changes in collagen fiber assembly and density in the dermis.

Table S2. Characterization of the wild type and *Adm*^{AM} haploinsufficient mice three days after the incision surgery: ability of the animals to move and gross findings from the skin tissue of the injured limbs.

Parameter measured		Before surgery		After surgery			Summary
		***Adm*$^{AM+/+}$**	***Adm*$^{AM+/\Delta}$**	***Adm*$^{AM+/+}$**	***Adm*$^{AM+/\Delta}$**	***Adm*$^{AM+/\Delta\ suppl.}$**	***Adm*$^{AM+/\Delta\ suppl.}$ *vs* *Adm*$^{AM+/\Delta}$**
		(n=4)	*(n=4)*	*(n=6)*	*(n=6)*	*(n=8)*	
Behavioral changes							
Animal ability to move	*good*	4	4	6		8	noticeable prevention
	impaired				6		
Anatomical changes							
Limb swelling		NS	NS	NS	severe	minor	noticeable amelioration
Histological changes							
Epidermis							
Thickness	*normal*	4	4	6		4	partial prevention
	increased				6	4	
Dermis							
Thickness	*normal*	4	4	6		4	partial prevention
	increased				6	4	
Erythrocyte extravasation		0	0	0	5	3	partial prevention
Inflammation [1]	*none*	4	4	6		4	partial prevention
	mild				6	4	

Incidence summary: total number of animals used for macroscopic and microscopic examination is indicated in brackets. NS - non-significant

[1]Note: lack of inflammation was considered if there was no: (1) bacterial infection; (2) pus; (3) warming or (4) redness of the skin; (5) bleeding (6) no aggregates of the inflammatory cells, including neutrophils; (7) no inflammatory cells in the lymphatic vessels.

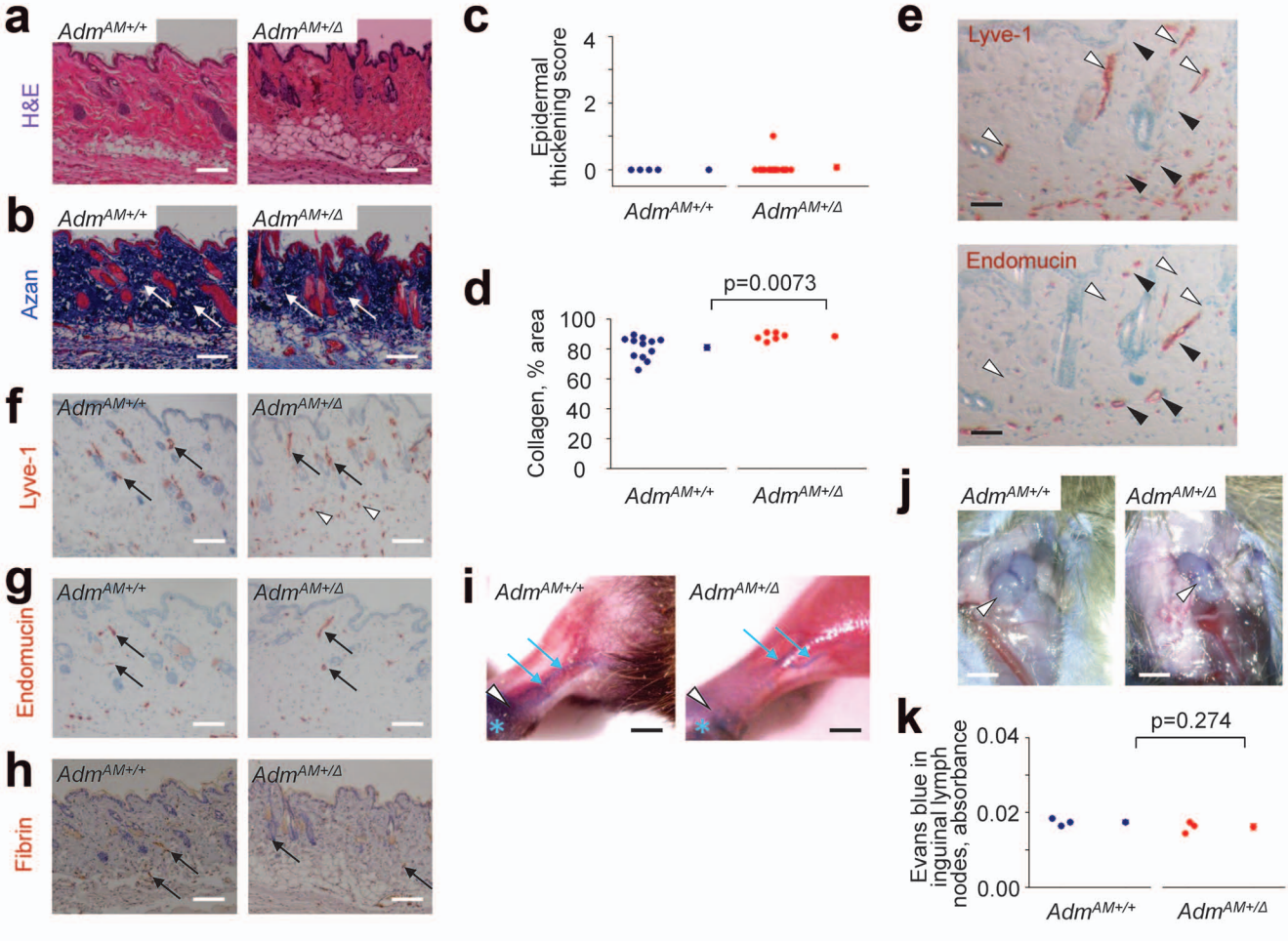

Figure S1. Comparative analysis of epidermis thickness, collagen deposition, lymphatic and blood vascular systems in the dermis, Evan blue uptake by collecting lymphatic vessels and its accumulation in inguinal lymph nodes were performed in the skin of an adult wild type (*Adm*$^{AM+/+}$) and *Adm*^{AM} haploinsufficient (*Adm*$^{AM+/\Delta}$) mice in physiological, i.e. unchalleneged, conditions. (**a**) The representative images of haematoxylin and eosin (*H&E*) and (**b**) Azan (*Azan*) staining are shown. Scale bars, 100 μm. Collagen fibers (*blue color; white arrows in* **b**) can be easily detected. (**c-d**) Quantitative data is presented as dot plots (left) alongside the mean and S.E.M. (right) for each experimental group. (**c**) The scoring of the epidermis thickness was performed in the skin samples from unoperated hind limbs from four wild type and thirteen *Adm*$^{AM+/\Delta}$ animals. (**d**) The area of collagen fibers in dermis of the skins in **b** was quantified and presented as percentage of the "signal/area" ratio. Comparisons between the groups were done using Welch two sample *t*-test. Actual p value is shown. (**e**) Characterization of the markers of lymphatic and blood vessel endothelium that were used to analyse microvascular system in the skin of the mice. Immunohistochemistry was performed on consecutive sections using antibodies against Lyve-1 (marker of lymphatic vessel endothelium; upper image; *brown color*) or endomucin (marker of blood vessel endothelial cells; lower image; *brown color*). Note mutually exclusive expression of endomucin and Lyve-1 in dermal lymphatic (*white arrowheads*) and blood (*black arrowheads*) capillaries respectively. Scale bars, 50 μm. (**f-g**) Immunoperoxidase staining (*brown color*) of the skin sections was performed using antibodies against (**f**) Lyve-1 (*black arrows*), (**g**) endomucin (*black arrows*) or (**h**) fibrin (used as a marker of plasma filtration and vascular leakage). Scale bars, 100 μm. Note that Lyve-1 positive macrophages (*white arrowheads*) are present in the skin of the *Adm*$^{AM+/\Delta}$ mice, and that the immunostaining for fibrin is restricted to the lumen of the dermal microvessels (*black arrows*) and absent in the interstitial space in the skin of both wild type and *Adm*^{AM} haploinsufficient mice. (**i**) To visualise collecting lymphatic vessels and to assess the interstitial fluid transport to the regional lymph nodes, intradermal injection of Evans blue into the footpad of the hind limb was done. Site of the dye injection is indicated with a *blue asterisk* and the knee - with a *white arrowhead* on representative images of unoperated hind limbs from mice from both experimental groups. Scale bars, 3 mm. Note that the lymphatic vessels are macroscopically visible (*blue arrows*) after Evans blue injection in mice from both experimental groups. (**j-k**) Evans blue uptake by inguinal lymph nodes was assessed in three mice in each experimental group. (**j**) Representative images of lymph nodes (*white arrowheads*) upon the uptake of the dye are shown. Scale bars, 1.5 mm. (**k**) Quantitative data for **j** is presented as dot plots (left) alongside the mean and S.E.M. (right). Comparisons amongst groups were done using *t*-test. Actual p value is shown. Note that the Evans blue uptake is unchanged in *Adm*^{AM} haploinsufficient mice, when compared to the wild type animals.

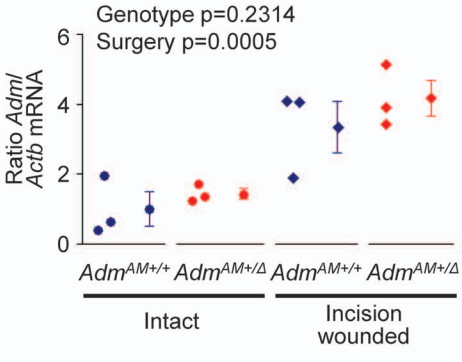

Figure S2. Adrenomedullin mRNA expression in the skin from non-operated (*Intact*) and skin incision wounded (*Incision wounded*) hind limbs from the adult wild type ($Adm^{AM+/+}$) and Adm^{AM} haploinsufficient ($Adm^{AM+/\Delta}$) mice was analysed by qRT-PCR. Ratio *Adm*/*Actb (β-actin)* was calculated to determine relative quantity of *Adm* mRNA. Quantitative data is presented as dot plots (left) alongside the mean and S.E.M. (right) for each experimental group. The comparisons amongst the groups were done using two-way ANOVA testing for effects of genotype (*Genotype*, i.e. $Adm^{AM+/+}$ or $Adm^{AM+/\Delta}$) and surgery (*Surgery*) independently (p values are shown in upper left corner). Note that *Adm* mRNA expression in both wild type and Adm^{AM} haploinsufficient mice is significantly (and to a similar magnitude) up-regulated in response to the incision wounding surgery; while the AM protein levels differ between the two experimental groups due to the abortive AM peptide translation from the mutant mRNA transcribed from the mutant locus in Adm^{AM} haploinsufficient mice (as shown on the Figure 1a and b in the main text).

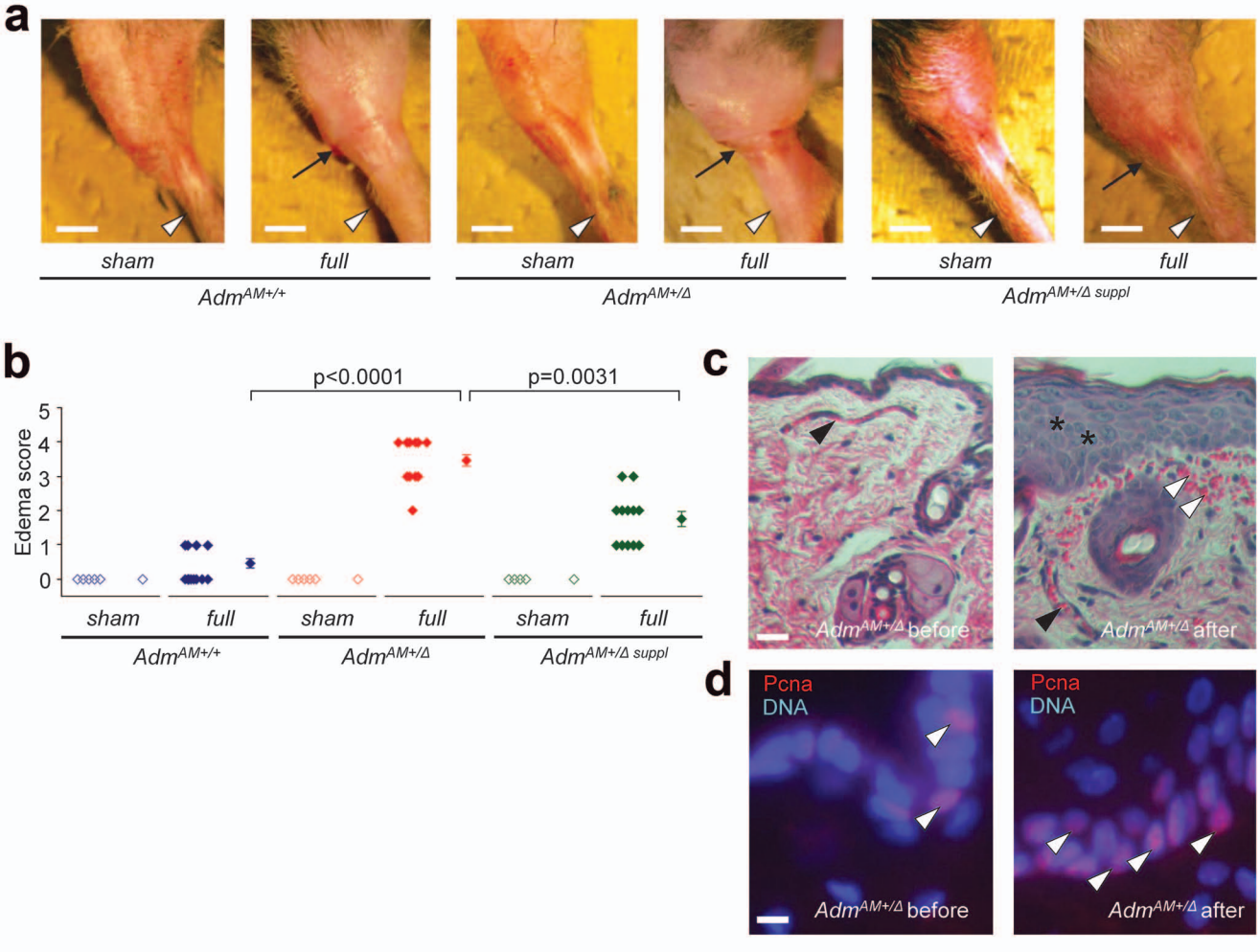

Figure S3. Edema and alterations in the skin of the adult adrenomedullin haploinsufficient mice three days after skin incision wounding. (**a-b**) Hind limbs of the wild-type (*Adm*$^{AM+/+}$) or *Adm* ^{AM} haploinsufficient mice without (*Adm*$^{AM+/\Delta}$) or with AM supplement (*Adm*$^{AM+/\Delta\ suppl}$) animals were either un-operated (i.e. shaved only; *sham*), or fully operated (*full*). (**a**) Representative images of the hind limbs from all experimental groups are shown (scale bars 5 mm). On each individual image, a *black arrow* is used to indicate the site of the surgery/injury (where relevant) and a *white arrowhead* – the knee. (**b**) The degree of the hind limb swelling was assessed three days after incision wounding by edema score in a blind fashion on a scale from 0 to 5. Data from five mice with sham-operated legs and from 15 mice with fully operated hind limbs is presented as dot plots (left) alongside the mean and S.E.M. (right) for each experimental group. Actual p values are shown. Comparisons amongst groups were done using Wilcoxon rank test. Note that the hind limb swelling is virtually absent in the sham operated legs of the mice in all three experimental groups, and that in fully operated hind limbs of *Adm*$^{AM+/\Delta}$ mice it is partially but significantly prevented upon AM peptide supplement. (**c**) Haematoxylin and eosin (scale bars, 25 μm) and (**d**) immunofluorescence staining (scale bars, 10 μm) of the skin of *Adm*^{AM} haploinsufficient mice before (*Adm*$^{AM+/\Delta}$ *before*) and after (*Adm*$^{AM+/\Delta}$ *after*) the incision wounding. (**d**) Immunofluorescence using anti-Pcna antibody and an appropriate Texas Red-conjugated (*red*) secondary antibody was performed to detect proliferating cells in the epidermis. DAPI (*blue*) was used to counterstain cell nuclei. Note (**c**) a thickened epidermis (*black asterisks*), erythrocytes extravasation (*white arrowheads*) as well as intact blood microvessels (*black arrowheads*) and (**d**) epidermal hyperplasia (*white arrowheads*) in the skin of the operated, when compared to unoperated, *Adm*^{AM} haploinsufficient mice.

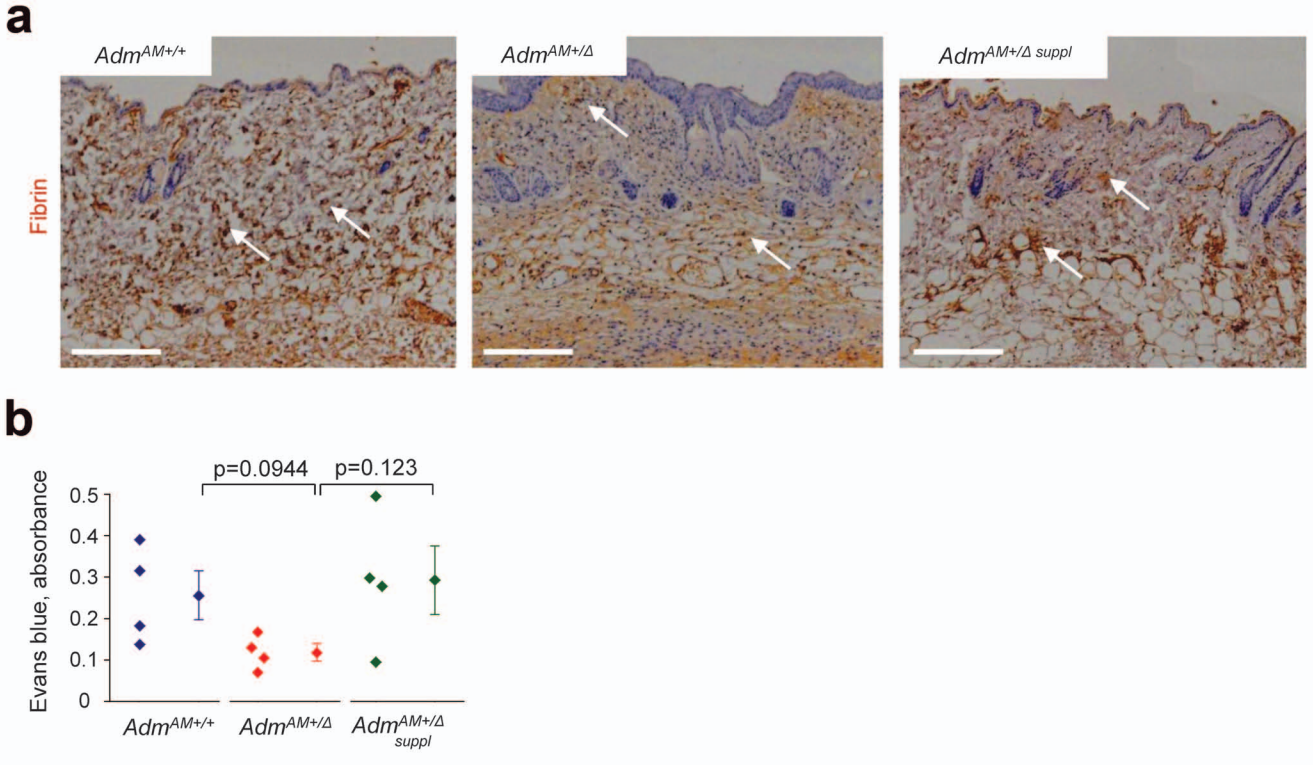

Figure S4. Alterations in the skin of the adult adrenomedullin haploinsufficient mice three days after skin incision wounding. Wild-type (*Adm*$^{AM+/+}$) or *Adm* ^{AM} haploinsufficient mice without (*Adm*$^{AM+/\Delta}$) or with AM supplement (*Adm*$^{AM+/\Delta\ suppl}$) animals were used for hind limb incision wounding. (**a**) Immunohistochemistry for fibrin was performed on skin sections at the same time as the immunostaining shown in the Supplementary Figure S1h. Representative images of the skin sections from operated legs from six to eight mice in each experimental group are shown (scale bars, 200μm). Note the increased diffuse immunoreactivity of the fibrin, reflecting its deposition, in the dermis (and in the extracellular space in particular; *white arrows*) and in the subcutaneous fat layer of mice from all three experimental groups after the surgery, when compared to mice before the surgery (see Supplementary Figure S1h). (**b**) Evans blue accumulation in operated hind limbs from four mice in each experimental group after intravenous administratuion. Comparisons amongst groups were done using Welch two sample *t*-test, with a two-tailed significance set at the 0.05 level and marginal significance set at the 0.1 level.

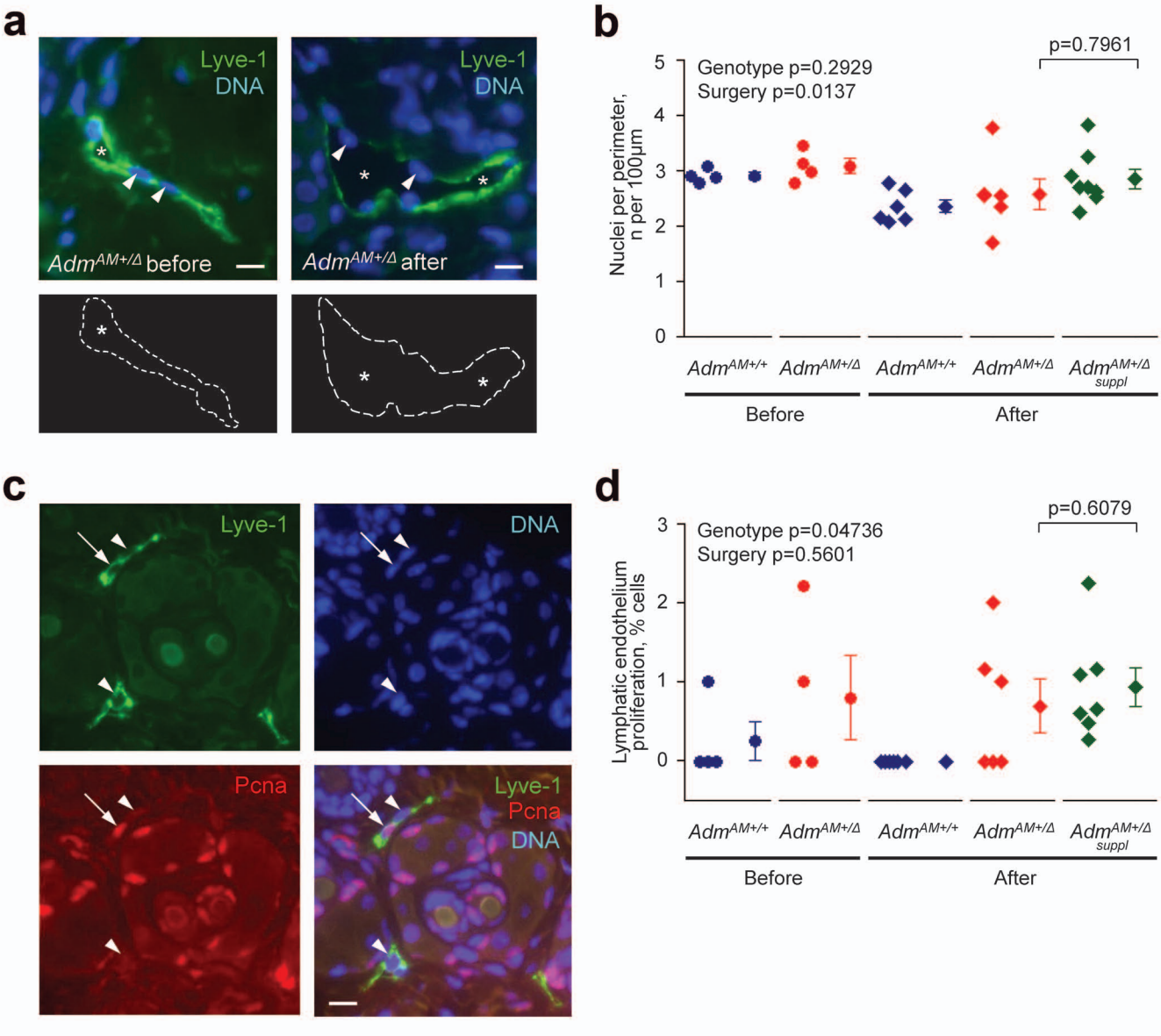

Figure S5. Endothelial cell number and proliferation in the lymphatic capillaries in the skin of *Adm*^{AM} haploinsufficient mice. Comparison of lymphatic endothelial cell **(a, b)** numbers per vessel perimeter or **(c, d)** their proliferation in the skins from wild-type (*Adm*$^{AM+/+}$) and from *Adm*^{AM} haploinsufficient mice without (*Adm*$^{AM+/\Delta}$) or with AM supplement (*Adm*$^{AM+/\Delta\ suppl}$); before (*Before*) or three days after (*After*) the hind limb skin incision wounding. **(a, c)** Lymphatic vessels were identified by immunofluorescence using anti-Lyve-1 (lymphatic endothelial cell marker) and an appropriate FITC-conjugated (*green*) secondary antibodies. DAPI (*blue*) was used to counterstain cell nuclei. Representative single color or merged images of the immunofluorescence staining are shown. Scale bars, 5 µm in **a** and 10 µm in **c**. **(a)** The perimeter of individual lymphatic vessels was defined as region of interest (ROI; lower images; *dotted lines*), and the **(b)** number of lymphatic endothelial cell nuclei (*white arrowheads*) per ROI was calculated. Vessels lumens are marked with *white asterisks*. **(c)** Anti-Pcna antibody and an appropriate Texas Red-conjugated (*red*) secondary antibody were used to detect proliferating cells in the skin. **(d)** The number of proliferating (*white arrow*) and non-proliferating (*white arrowheads*) lymphatic endothelial cells was calculated based on double immunofluorescence data for both Lyve-1 and Pcna. **(b, d)** Quantitative data in the skin from operated hind limbs in four to eight mice mice from all experimental groups is presented as dot plots (left) alongside the mean and S.E.M. (right). Note that the data for the groups before hind limb surgery is shown for the direct comparison with post incision wounding conditions. The comparisons amongst the first four groups were done using two-way ANOVA testing for effects of genotype (*Genotype,* i.e. *Adm*$^{AM+/+}$ or *Adm*$^{AM+/\Delta}$) and incision wounding (*Surgery*) independently (p values are shown in upper left corner), followed by Welch two-sample *t*-test for groups 4 and 5 (*Adm*^{AM} haploinsufficient mice with or without AM supplement; p value is shown in upper right corner).

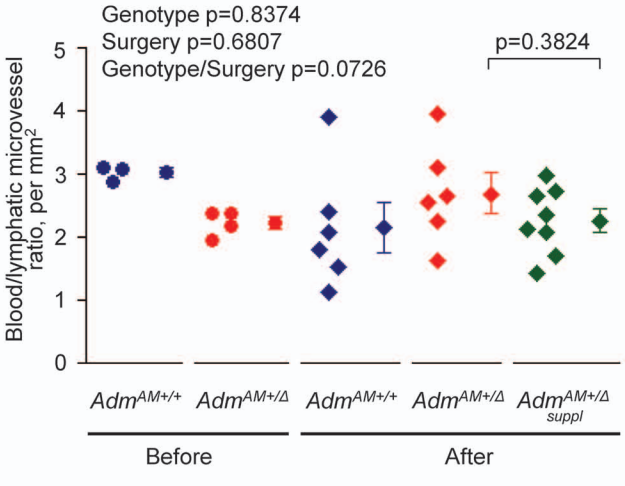

Figure S6. Blood/lymphatic microvessel number ratio in the skin was calculated by dividing numbers obtained for each vessel type for each experimental group, including adult wild-type ($Adm^{AM+/+}$) and Adm^{AM} haploinsufficient mice without ($Adm^{AM+/\Delta}$) or with an exogenous AM supplement ($Adm^{AM+/\Delta\ suppl}$). Quantitative data from four to eight mice in each group under normal physiological conditions or three days after the incision wounding surgery is presented as dot plots (left) alongside the mean and S.E.M. (right). The values for the experimental groups before the surgery are shown for direct comparison with post incision wounding conditions. The comparisons amongst the first four groups were done using two-way ANOVA testing for effects of genotype (*Genotype,* i.e. $Adm^{AM+/+}$ or $Adm^{AM+/\Delta}$) and surgery (*Surgery*) independently; where it was suggested by the plots and data, we also tested possible interactions between these factors (i.e. whether the effect of genotype was different after surgery to before; *Genotype/Surgery*) (p values are shown in upper left corner), followed by Welch two-sample *t*-test for groups 4 and 5 (Adm^{AM} haploinsufficient mice with or without AM supplement; p value is shown in upper right corner).

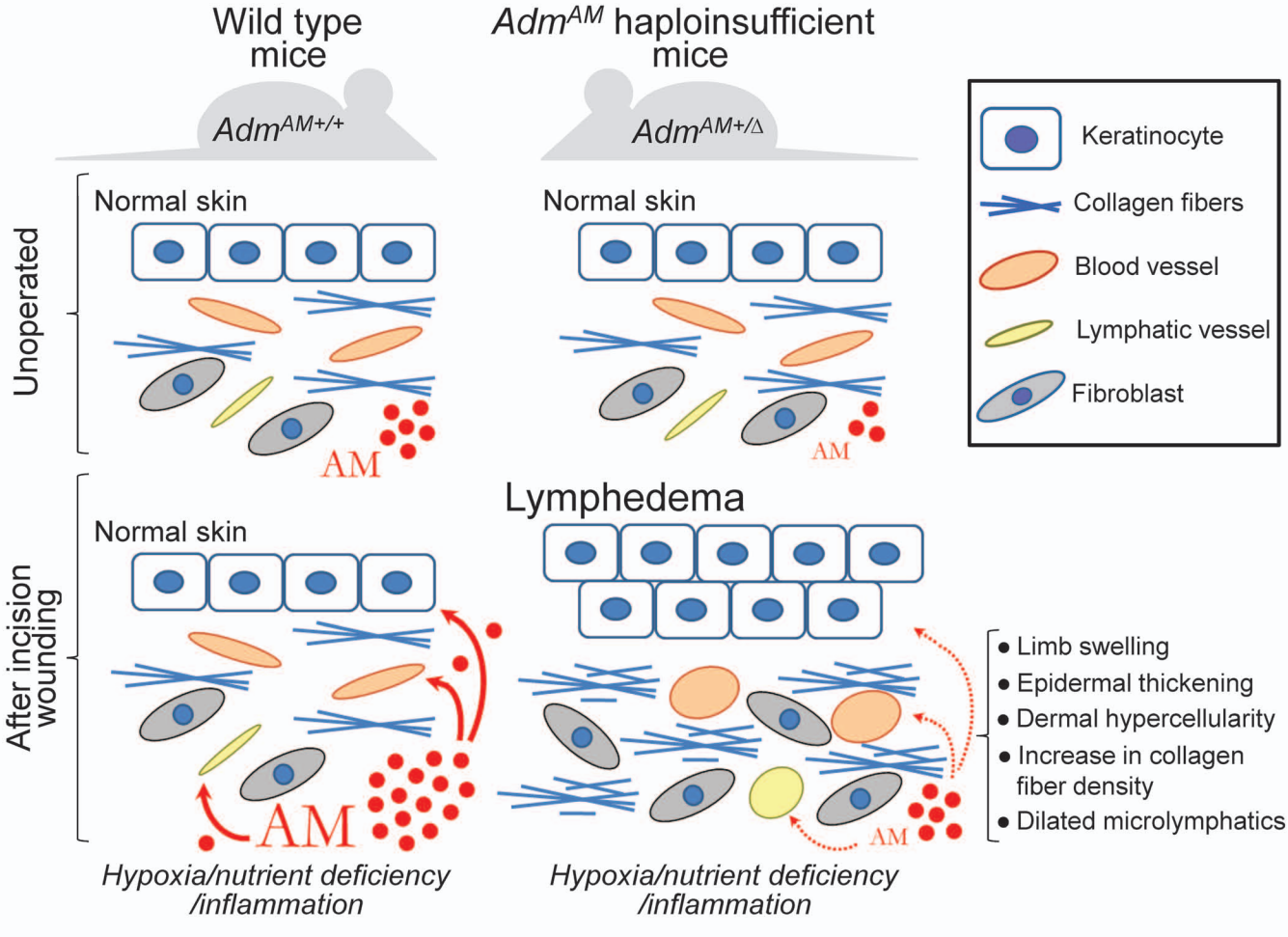

Figure S7. The proposed model of the role for peptide adrenomedullin in the pathogenesis of the secondary lymphedema upon hind limb skin incision wounding surgery in mice. Endogenous expression of adrenomedullin (AM) is up-regulated in the skin upon incision wounding and prevents lymphedema development in wild type mice (*left panel*), while *Adm*^{AM} haploinsufficiency (resulting in AM deficiency) causes lymphedema (*right panel*). Note that the development of the secondary lymphedema in *Adm*^{AM} haploinsufficient mice was prevented, when circulating AM levels were restored by peptide supplementation, suggesting that endogenous AM signaling is directly involved in the pathogenesis of this disorder.

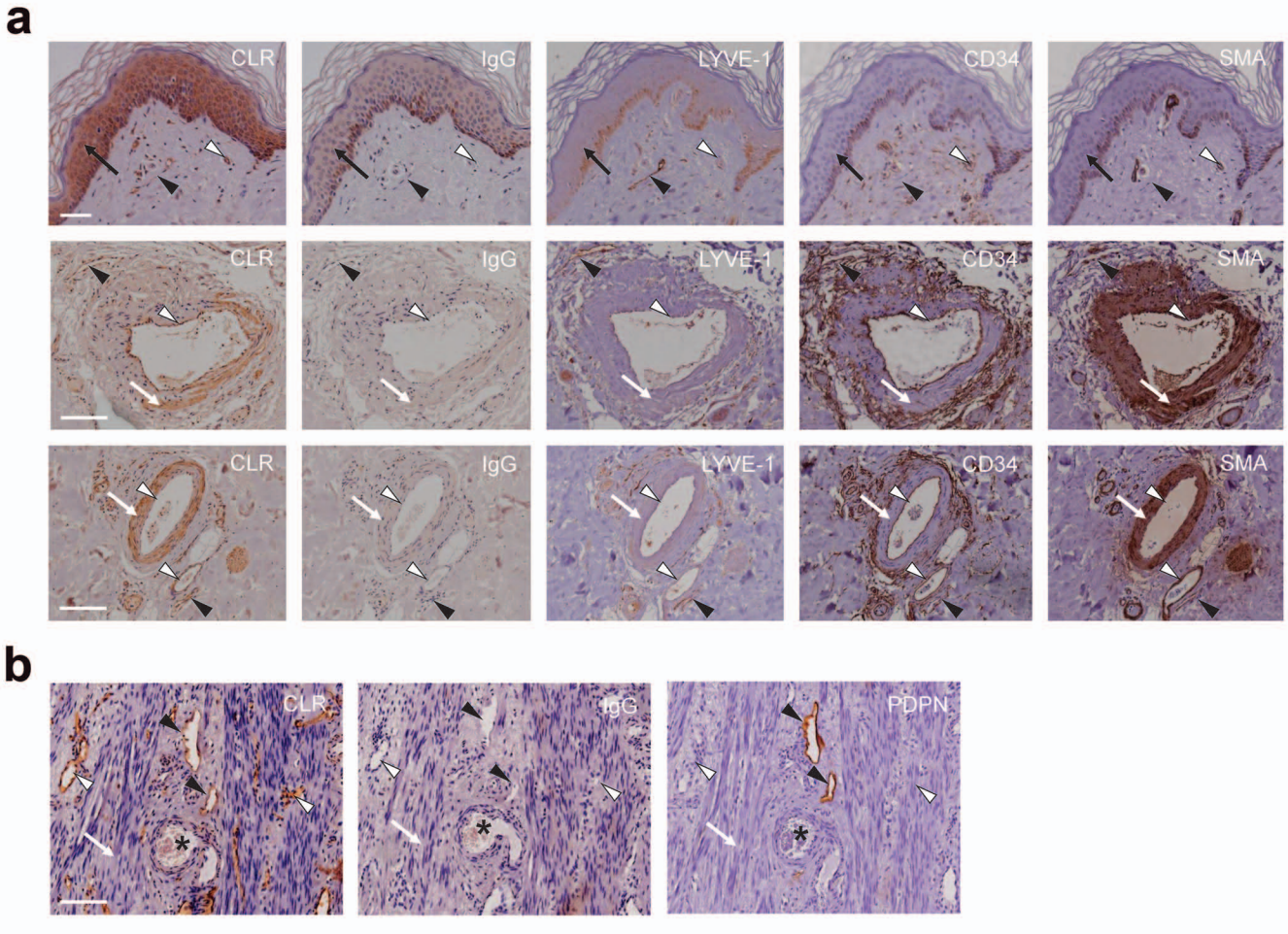

Figure S8. CLR expression and localisation in human tissues. CLR distribution n serial sections from human (**a**) skin and (**b**) myometrium was analysed by immunohistochemistry using polyclonal anti-human CLR (CLR) antibody LN1436 (3). Antibodies raised against CD34 (blood vessel endothelium marker; CD34), LYVE-1 (lymphatic endothelium marker; LYVE-1), podoplanin (lymphatic endothelium marker; PDPN) and alpha smooth muscle actin (vascular smooth muscle cell marker; SMA) or appropriate control immunoglobulins (IgG) were also used. Signal was revealed by using DAB (*brown color*). Sections were stained with haematoxylin to visualize the cell nuclei (*blue color*). (**a**) Top panel – scale bar, 100 µm; middle and bottom panels – scale bars, 50 µm. Note that in the skin, CLR is expressed in keratinocytes (*black arrows*), lymphatic (*black arrowheads*) and blood (*white arrowheads*) microvessel endothelium, and to some extent in smooth muscle cells (*white arrows*) around larger vessels. (**b**) Scale bar, 100µm. Note that in the myometrium, CLR is expressed in the endothelium of both podoplanin-positive lymphatic (*black arrowheads*), as well as podoplanin-negative blood (*white arrowheads*) microvessels, and not in larger vessels (*asterisk*) or smooth muscle myometrial cells (*white arrows*).

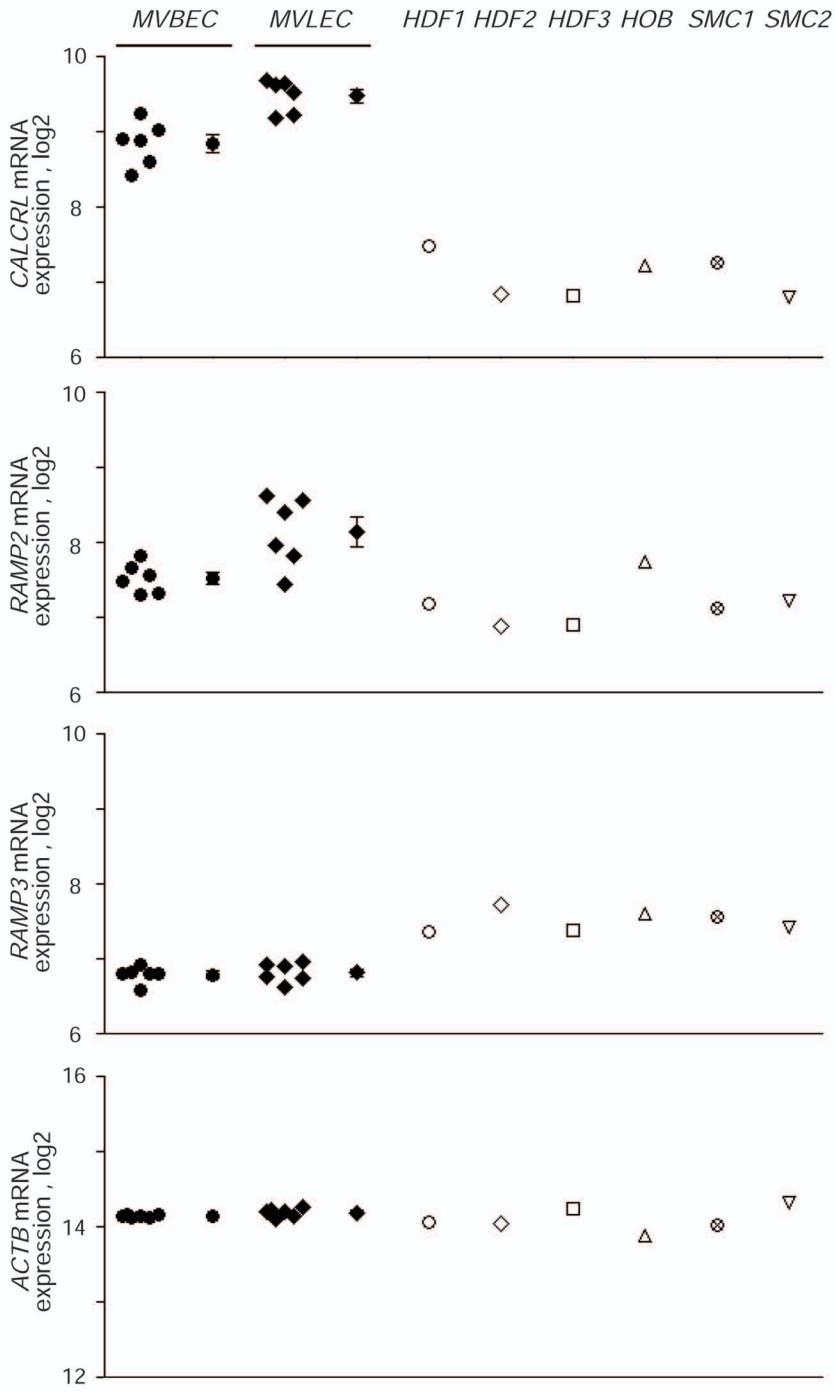

Figure S9. *CALCRL* and *RAMPs* expression in primary human cells. The analysis of *CALCRL, RAMP2, RAMP3 and ACTB* mRNA expression was performed using GeneChip® Human Genome array data (E-MEXP-66 and GSE39262; mean values 'rma' $\log_2$ expression units for the probes 210815_s_at, 205779_at, 205326_at and 200801_x_at respectively) obtained from dermal microvascular blood and lymphatic endothelial cells (*MVBEC* and *MVLEC* respectively; six cell isolates for each), dermal fibroblasts (*HDF*; isolates 1-3), HOB – osteoblasts, SMC – smooth muscle cells (isolate 1 – from penile tissue, isolate 2 – from myometrial tissue). Quantitative data for each group of endothelial cell isolates is presented as dot plots of individual values (left) alongside the mean and S.E.M. (right; both – *black symbols*), and for other cell types - as individual values (all – *white symbols*).

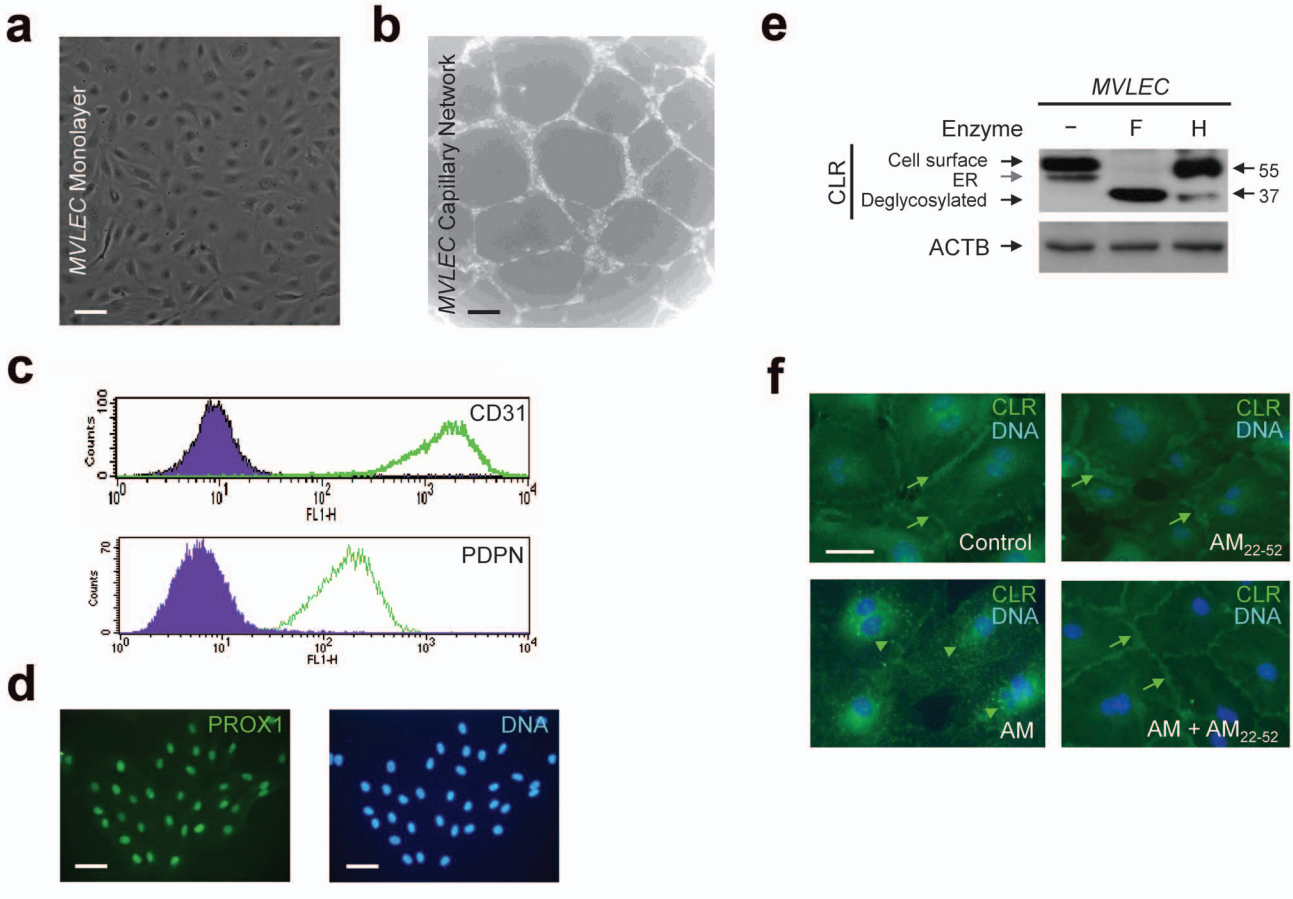

Figure S10. CLR expression in cultured human primary lymphatic endothelial cells from dermal microvessels. (a) Isolated primary microvessel lymphatic endothelial cells (*MVLEC*) formed the monolayer on attachment factor-coated dishes and **(b)** the capillary network, when seeded on Matrigel. **(c)** Endothelial origin of the primary human MVLEC cultures was confirmed by FACS analysis of the CD31 (CD31; *green line*) as a pan-endothelial marker and podoplanin (PDPN; *green line*) as a marker of lymphatic endothelial cells. Isotype-matched mouse IgG and pre-immune rabbit serum were used as appropriate controls (*shaded purple areas*) for the FACS analysis with anti-CD31 and anti-podoplanin antibodies respectively. **(d)** MVLEC were immunostained with monoclonal anti-PROX1 antibody and appropriate FITC-conjugated secondary antibody. DAPI (*blue*) was used to counterstain cell nuclei. Expression of PROX1 homeobox transcription factor (*green*), known as a marker of endothelial cells of lymphatic lineage, was observed virtually in the whole population of the primary MVLEC. **(e)** Expression of endogenous CLR species in MVLEC was analyzed by immunoblotting using polyclonal antibody LN1436 which recognizes deglycosylated, core-glycosylated and terminally-glycosylated forms of the receptor (Nikitenko et al., 2006a). Protein lysates were treated with endoglycosidase F (*F*), endoglycosidase H (*H*) or no enzyme (–) before SDS-PAGE under reducing conditions and immunoblotting with polyclonal anti-human CLR antibody LN1436. *Arrows*, deglycosylated (~37 kDa; *black arrow*), core-glycosylated (~45 kDa; ER-associated form; *grey arrow*) and mature (fully or terminally; cell surface-associated form; *black arrow*) glycosylated (~55 kDa) forms of the receptor. The ~55 kDa CLR species are reduced to a ~37 kDa CLR band after endoglycosidase F treatment, but are resistant to endoglycosidase H. For loading controls, the membrane was re-probed with an antibody against human beta actin (*ACTB*). **(f)** The interaction of the endogenous CLR expressed in primary human MVLEC with AM peptide. Subcellular distribution of endogenous CLR in MVLEC before treatment (Control) and after exposure to AM (AM, 100 nM for 15 minutes) with or without antagonist (AM_{22-52}, 1 μM) was assessed by immunofluorescence using LN1436 primary and FITC-conjugated secondary antibodies. DAPI was used to counterstain cell nuclei. Figures are representative merged images of two independent experiments. Cell surface (noticeable in cell-cell contacts; *green arrows*) and internalized (punctuate staining; *green arrowheads*) endogenous CLR species are indicated. Internalized CLR is contained within early endosomes, as confirmed by its co-localization with early endosome antigen (EEA1) (not shown).